

Article

Line Force and Damping at Full and Partial Stator Overlap in a Linear Generator for Wave Power

Liselotte Ulvgård ^{*,†}, Linnea Sjökvist [†], Malin Göteman and Mats Leijon

Department of Engineering Sciences, Uppsala University, Box 534, Uppsala 751 21, Sweden;
linnea.sjokvist@angstrom.uu.se (L.S.); malin.goteman@angstrom.uu.se (M.G.);
mats.leijon@angstrom.uu.se (M.L.)

* Correspondence: liselotte.ulvgard@angstrom.uu.se; Tel.: +46-18-471-5843

† These authors contributed equally to this work.

Academic Editor: Raúl Guanche García

Received: 30 June 2016; Accepted: 16 November 2016; Published: 28 November 2016

Abstract: A full scale linear generator for wave power has been experimentally evaluated by measuring the line force and translator position throughout the full translator stroke. The measured line force, in relation to translator speed, generator damping and stator overlap, has been studied by comparing the line force and the damping coefficient, γ , for multiple load cases along the translator stroke length. The study also compares the generator's behavior during upward and downward motion, studies oscillations and determines the no load losses at two different speeds. The generator damping factor, γ , was determined for five different load cases during both upward and downward motion. The γ value was found to be constant for full stator overlap and to decrease linearly with a decreasing overlap, as the translator moved towards the endstops. The decline varied with the external load case, as previously suggested but not shown. In addition, during partial stator overlap, a higher γ value was noted as the translator was leaving the stator, compared to when it was entering the stator. Finally, new insights were gained regarding how translator weight and generator damping will affect the translator downward motion during offshore operation. This is important for power production and for avoiding damaging forces acting on the wave energy converter during operation.

Keywords: wave power; force measurement; line force; power take-off; damping

1. Introduction

1.1. Background

Many different power takeoff (PTO) systems have been studied and tested for converting wave power to electricity [1–9]. At Uppsala University, prototypes of generators, point absorber buoys and marine substations have been tested and evaluated in full scale at the offshore research site in Lysekil, Sweden, since 2006. The wave energy converter (WEC) concept considered uses a permanent magnet linear generator placed at the ocean bed, which is directly coupled with, and driven by, a point absorbing buoy [10]. The translator is lifted by the buoy in the wave peaks, while gravity acts as the retracting force in the wave troughs. The translator is held in place and guided by wheel-tracks mounted to the hull of the generator. Throughout the full translator stroke, the generator will have a varying active area, A_{fac} , which is the ratio between the stator–translator overlap and the total stator area, as shown in Figure 1. The expected PTO force during full stator overlap, when neglecting mechanical and electrical losses, has been derived in theory [11] and simulated [12], but it has not been studied experimentally for this WEC. How the force changes with decreasing stator overlap is not yet fully explored, neither in theory nor experiment [13].

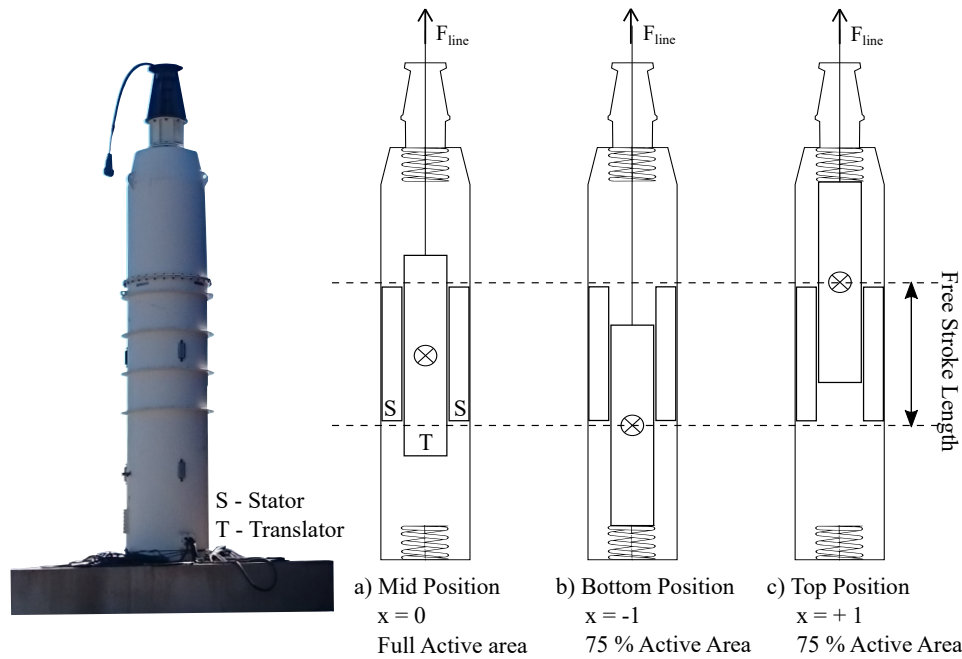


Figure 1. The L10 generator and a sketch of it with the translator at (a) mid position, which full stator overlap; (b) the lower endstop, where $A_{fac} = 75\%$; and (c) at the upper endstop, where $A_{fac} = 75\%$. It should be noted that the endstops can be compressed, which makes translator positions beyond the free stroke length possible.

The force in the line, connecting the buoy to the translator, decides the mechanical input power that is transferred to the generator during normal operating conditions [14]. During storms and extreme waves, this is also the limiting force to consider for the structural design of the WEC [15,16]. The endstop force, i.e., the peak line force when the translator hits the upper endstop, is the critical design force. For the WEC concept considered, the line force has been measured offshore in both full scale during normal operating conditions [17,18] and in a scaled model, with linear springs instead of a PTO, in larger seas [19]. However, the offshore environment does not provide the controlled environment needed to make a qualitative analysis. In a 1:20 scale experiment performed in a wavetank, the endstop force was measured for normal operating conditions and for extreme waves. Frictional damping was used as PTO-damping, which was varied, and it was found that the endstop force decreased by an increased PTO-damping [20].

An important phenomenon that has been observed during offshore operation of a similar WEC, named L9, is that more power was generated during the upward motion of the translator than during the downward motion [21]. It was concluded that this behavior was due to a lower translator speed in the downward stroke, when gravity is the only retracting force. To improve the retracting force, and thereby increase translator speed and power output, the translator mass in the L10 prototype, studied in this paper, was increased compared to the prototype studied in reference [21].

1.2. Paper Objective

In this study, onshore generator tests were performed in order to measure and evaluate the line force throughout the full stroke of the translator, including the full active area, partial active area and during endstop hits. The line force is expected to vary with translator position, mechanical frequency (generator speed) and PTO damping. The study also compares the generator’s behavior during upward and downward motion, studies oscillations during the stroke and calculates the no load losses at two different speeds.

The data was studied by comparing the measured line force for different load cases along the translator stroke length and by calculating and comparing the damping coefficient γ , for each load

case, along the stroke length. Previous measurement of the damping coefficient γ has been made for the full active area [22,23], but then based on power output. By retrieving γ from measured line force data, instead of electrical output, a better measure of the forces acting on the generator and buoy is provided. This gives a a better understanding of the dynamical behavior of the WEC. The paper also show how γ decreases with decreasing active area.

Onshore generator testing does not provide the same force dynamics as sea trials, but by studying the generator's onshore behavior in a controlled test environment, its behavior during offshore operation can be better understood and predicted.

2. Method

2.1. WEC Dynamics

The dynamic behavior of the WEC during offshore operation is described by the equations of motion. The translator and buoy are connected by the line force F_l , which drives the motion of the translator. The dynamics of the buoy is determined by its equation of motion (1) and the translator motion (2). When the line slacks, F_l turns to zero and the buoy and translator will move independently of each other until the line is stretched again:

$$(m_a^\infty + m_b)\ddot{x}_b(t) = \int PdS - \rho gV(x_b) - m_b g - F_l \tag{1}$$

$$m_t \ddot{x}_t(t) = F_l \pm F_{PTO} - m_t g \pm F_{loss}^{fric} \pm F_{endstop} \tag{2}$$

The added mass at infinity, buoy mass and translator mass are described by m_a^∞ , m_b and m_t , respectively. In Equation (1), $\int PdS$ and $\rho gV(x_b)$ represent the hydrodynamic and the hydrostatic force, where $V(x_b)$ is the submerged volume and ρ the water density. The PTO force will work in the opposite direction of the translator motion and is:

$$F_{PTO} = \gamma \dot{x}_t(t) \tag{3}$$

where γ is a damping coefficient, dependent on translator speed, external load and active area A_{fac} (i.e., the translator position). F_{PTO} will include electrical losses in the generator, which can be divided into copper losses, F_{loss}^{Cu} , and iron losses, F_{loss}^{Fe} [24]. The copper losses depend on the current and the resistance in the stator windings; they are independent of translator speed. When no load is connected to the generator, there will be no copper losses. The iron loss is a sum of hysteresis loss, eddy current loss and excess loss, and is dependent on both load and electrical frequency (i.e. translator speed). The speed dependence, $F_{loss}(x_t^m)$, will depend on the distribution between hysteresis, eddy current and excess loss, so that m will be a number between 1 and 2.

The frictional losses are described by F_{loss}^{fric} . The total friction in the studied WEC is a sum of lubricated friction from the mechanical lead-through, dependent on speed and lubricant viscosity, and a rolling resistance from the wheel-tracks, which, in an ideal case, has a very small speed dependence [25]. However, the visco-elasticity of the rubber coating of the wheels can introduce an increased speed dependence. In the no load case, when there will be no power production and no copper losses, it is possible to extract the sum of the friction and the iron losses at no load:

$$F_{loss}^{fric} + F_{loss}^{Fe(noload)} = (F_{line-up} - F_{line-down})/2 \tag{4}$$

In a balanced generator, the iron losses at no load will be small and the greater part of the no load losses will be frictional loss [26].

2.2. Experimental Set-Up

The generator studied, L10, is shown in Figure 1 and the specifications can be found in Table 1. Due to changes made during translator assembly, the active area decreased to 65% in the top position, instead of the designed value presented in Figure 1c. The generator internal resistance was measured to 1.2 Ω per phase. The self-inductance for each phase is 19.3 mH, measured with the translator in the bottom position. Phase shift between voltage and current was measured to confirm that the inductance is negligible compared to the generator resistance throughout the full stroke. During the tests, measurements were made of the line force, phase voltages and currents. The measurement equipment is listed in Table 2. All signals were logged simultaneously at 250 Hz with a data acquisition module, CompactRIO 9205.

Five load cases were tested: no load, 6.6 Ω, 4.4 Ω, 2.2 Ω and short circuit, as presented in Table 3. It should be noted that a higher load resistance will result in a lower PTO damping. During tests, the translator was lifted until hitting the upper endstop, and then lowered again, with the same speed. This was repeated for a high and low lift speed, for each load case. Care was taken to keep the speed constant to the greatest extent possible, considering that a crane is an imprecise tool. The crane lifting procedure is controlled by speed, but limited by power, which limited the possibility to keep a high and constant speed during high PTO damping in run 7 to run 10. Due to the high PTO force in run 8 to run 10, the crane operator could not distinguish the increased force when the endstop was hit, but reversed the direction of the crane before the endstop was hit.

Table 1. Generator specifications for the L10 generator, at rated speed 0.7 m/s.

Parameter	Symbol	Value
Nominal power	P_{nom}	20 kW
Main RMS voltage	V_{RMS}	450 V
Free stroke-length	l_{free}	2 m
Translator length	$l_{translator}$	2.8 m
Translator mass	$m_{translator}$	6350 kg
Stator length	l_{stator}	2 m
Upper endstop-spring constant	κ	250 kN/m

Table 2. Measurement equipment and their accuracies.

Equipment	Accuracy
Force transducer -Sensy 5050 Load pin	Linearity error: $< \pm 1\%F.S. = \pm 500$ kg Repeatability error: $< 0.25\%F.S. = \pm 125$ kg Zero shift after loading: $< \pm 0.05F.S = \pm 25$ kg
Differential voltage probes - TESTEC TT-SI 9001	$\pm 2\%$
Current probes -Fluke i310s	$\pm 1\%$ at range ± 300 mA
Data acquisition -NI9205	6.23 μV at range ± 10 V 690 μV at range ± 1 V

Table 3. Test setup.

Experiment Case		Resistive Load	Endstop Hit?
run 1	low speed	no load	yes
run 2	-	6.6 Ω	yes
run 3	-	4.4 Ω	yes
run 4	-	2.2 Ω	yes
run 5	-	short circuit	yes
run 6	high speed	no load	yes
run 7	-	6.6 Ω	yes
run 8	-	4.4 Ω	no
run 9	-	2.2 Ω	no
run 10	-	short circuit	no

2.3. Post Processing of Data

The translator motion was calculated from the generator output voltage, knowing that the distance between two zero-crossings in the voltage signal corresponds to one pole-width of the linear generator. The derived position data was interpolated to achieve the same sampling frequency as in the measured signals, using a piecewise cubic interpolation method. This method was validated by comparing the derived position curve with the sinusoidal shape of the voltage signal, knowing the expected signal shape at constant speed. A similar method is presented in more detail in reference [27]. It should be noted that since both upper and lower endstop will be compressed at translator impact, the full stroke length is longer than the free stroke length of ± 1 m. The speed was derived from the position data using numerical differentiation.

It is of interest to relate the time sampled force data directly to the position data, in order to compare line force during upward and downward strokes at the same translator position. This was done by splitting each data set at the maximum position and then cross referencing the downward motion data to the upward motion data, symmetrically about the maximum position.

To identify and evaluate force oscillations, fast fourier transform (FFT) was used in both time and position domain. In order to perform FFT in the position domain, the position-referenced force data was interpolated to a constant sampling frequency.

For readability, the line force data used for Figures 1–7 has been digitally filtered with a low-pass Butterworth filter. Motivated by the measured line force noise at translator standstill, the cut-off frequency was set to 8 Hz. The electrical frequency of the generator is 0.1 Hz and 1 Hz for the two studied speed cases.

3. Results

3.1. Measured Line Force as a Function of Time

Figure 2 presents the measured line force, position and speed for all load cases during the low speed tests. Figures 3 and 4 show the same for the high speed tests. The endstop hit is seen as a line force peak between the upward and downward stroke. Comparing the line force for each load case at different speeds, it can be concluded that a higher speed gives a higher line force, both at endstop hits and during the full active area. Table 4 summarizes the line force and speed measured for each load case during full active area, for both upward and downward strokes, and at upper endstop impact.

The boxed areas in Figures 2c, 3c and 4c marks out the speed during the full active area. In the low speed tests, all load cases show similar and rather constant speeds during both strokes, matched as well by constant line forces. In the high speed tests, the speeds differ more between the load cases, but are still stable within the full active area during the upward stroke.

The no load case shows strong oscillations in both Figures 2 and 3, which is also mirrored in the line force data in Figure 2a. These oscillations are evaluated further in Section 3.2.1.

The high speed short circuit case is presented separately in Figure 4. The translator held a speed of only 0.14 m/s when moving upwards, due to high generator damping and limitations in the crane. It should be noted that the measured line force for the short circuit case would be significantly higher if the same speed had been achieved as for the other load cases. When lowered down, starting at about $t = 20$ s, the measured line force drops to zero, which means that there is a slack in the line. Thus, the downward motion of the translator is damped only by the generator damping until $t = 25\text{--}40$ s when the weight is shifted over to the crane again. From $t = 40$ s, the translator moves down to its bottom position. Line slack can also be seen in the 2.2Ω case, in Figure 3a, where the measured line force drops to zero at a point where the translator has only reached mid position.

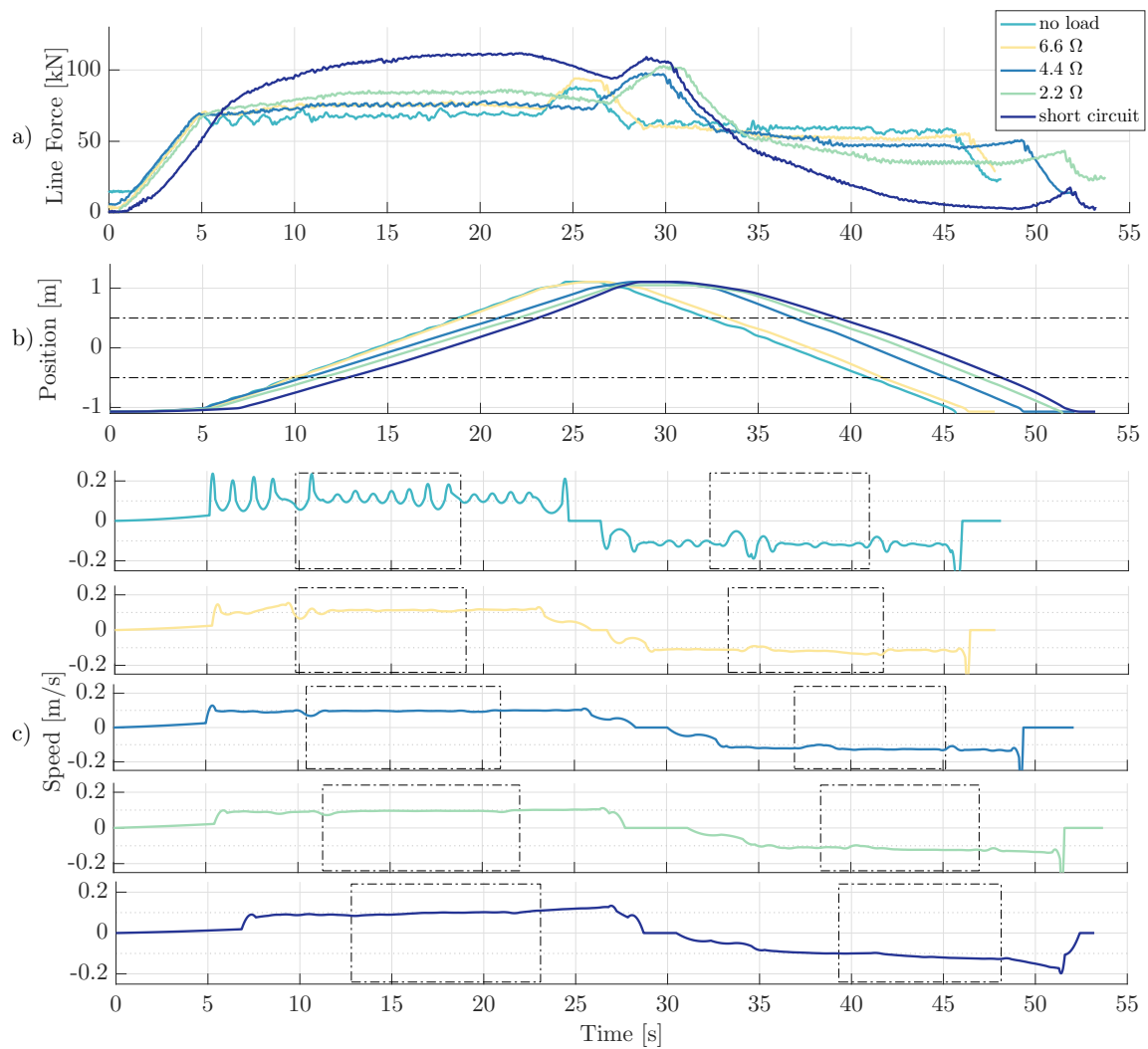


Figure 2. Measured line force (a), translator position (b) and translator speed (c) in time domain for the low speed tests. Dotted areas mark out full active area.

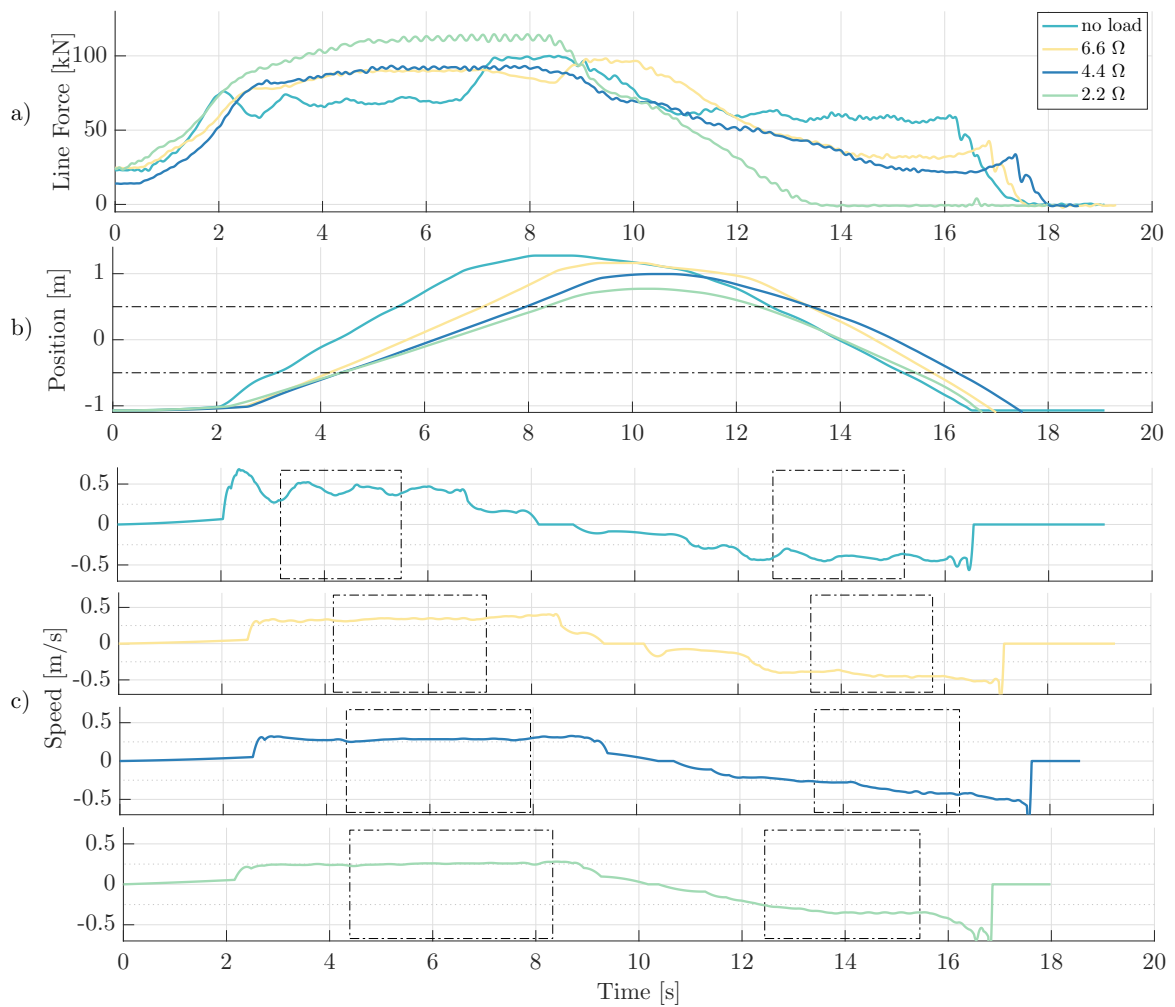


Figure 3. Measured line force (a), translator position (b) and translator speed (c) in time domain for the high speed tests. Dotted areas mark out full active area.

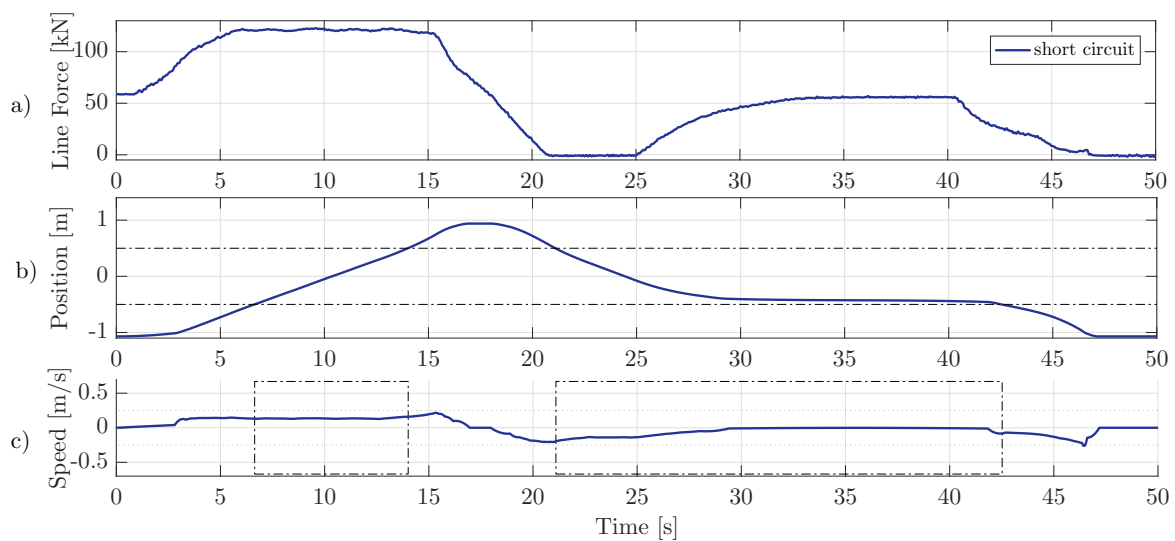


Figure 4. Measured line force (a), translator position (b) and translator speed (c) for the short circuit case during the high speed stroke. Dotted areas mark out full active area.

Table 4. Measured line force during the full active area and at upper endstop impact. The line force and speed during the full active area is presented with average value and standard deviation, *s*, for the data corresponding to the dotted boxes in Figures 2c, 3c and 4c.

Load Case	Speed up (m/s)	Line Force up (kN)	Speed down (m/s)	Line Force down (kN)
Average line force and speed at the full active area-low speed				
no load	0.11 (<i>s</i> = 0.03)	68.0 (<i>s</i> = 1.7)	0.12 (<i>s</i> = 0.03)	59.5 (<i>s</i> = 1.8)
6.6 Ω	0.11 (<i>s</i> = 0.01)	75.5 (<i>s</i> = 0.9)	0.11 (<i>s</i> = 0.01)	53.5 (<i>s</i> = 1.6)
4.4 Ω	0.10 (<i>s</i> = 0.01)	75.7 (<i>s</i> = 0.9)	0.12 (<i>s</i> = 0.01)	48.2 (<i>s</i> = 1.9)
2.2 Ω	0.09 (<i>s</i> = 0.01)	84.0 (<i>s</i> = 1.0)	0.12 (<i>s</i> = 0.01)	37.0 (<i>s</i> = 2.9)
short circuit	0.10 (<i>s</i> = 0.01)	109.2 (<i>s</i> = 2.2)	0.11 (<i>s</i> = 0.01)	9.4 (<i>s</i> = 5.6)
Average line force and speed at the full active area-high speed				
no load	0.43 (<i>s</i> = 0.05)	67.0 (<i>s</i> = 2.1)	0.39 (<i>s</i> = 0.04)	58.8 (<i>s</i> = 1.7)
6.6 Ω	0.34 (<i>s</i> = 0.01)	89.6 (<i>s</i> = 0.9)	0.42 (<i>s</i> = 0.03)	34.3 (<i>s</i> = 3.3)
4.4 Ω	0.28 (<i>s</i> = 0.01)	91.6 (<i>s</i> = 1.2)	0.36 (<i>s</i> = 0.06)	28.1 (<i>s</i> = 6.2)
2.2 Ω	0.25 (<i>s</i> = 0.01)	111.3 (<i>s</i> = 1.8)	0.33 (<i>s</i> = 0.03)	n/a ^a
short circuit	0.136 (<i>s</i> = 0.01)	121.3 (<i>s</i> = 0.7)	0.04 (<i>s</i> = 0.06)	n/a ^a
Load Case	Speed before Endstop Hit (m/s)		Peak Force (kN)	
Line force peaks at low speed				
no load	0.112		88.36	
6.6 Ω	0.119		94.49	
4.4 Ω	0.103		97.93	
2.2 Ω	0.104		102.2	
short circuit	0.127		109.3	
Line force peaks at high speed				
no load	0.423		99.08	
6.6 Ω	0.403		98.06	

^a Not applicable due to line slack.

3.1.1. Line Force Dependence of PTO Damping

Figures 2a, 3a and 4a show that the line force becomes higher with higher damping, both at the endstop and during mid-stroke, which is to be expected. The peak forces are presented in Table 4 together with translator speed just before endstop impact. For the faster strokes, only the no load case and the 6.6 Ω case show clear endstop hits.

There is a distinct drop in line force before the endstop for all cases except at no load. A corresponding line force peak can be seen during the downward stroke just before the bottom endstop. This is mainly due to decreasing active area, which decreases the PTO force. The decrease in line force before the upper endstop is also matched by a small increase in speed in the short circuit case, which is a reasonable consequence when the crane experiences a lower force.

In the short circuit and 2.2 Ω load cases presented in Figures 3 and 4, the translator speed during freefall is measured, when there is no line force. This is the highest downward speed achievable for the generator at this load. At short circuit, the translator almost reached a standstill, while the 2.2 Ω held a speed of 0.35 m/s, similar to the other load cases. It should be noted, though, that the rated generator speed is 0.7 m/s.

3.2. Measured Line Force as a Function of Translator Position

Figures 5 and 6 show the same data as Figures 2 and 3, but with upward and downward strokes presented together along the stroke length. Solid lines represent the upward stroke, from bottom position to upper endstop, and dotted lines represent the downward stroke. The vertical dotted lines represent the position, where the stator is fully overlapped by the translator and the active area is full, $A_{fac}(x) = 1$.

The upward strokes show a higher line force than the downward stroke. This is due to the direction of the PTO force, which will work in the opposite direction of the line force during the upward stroke and in the same direction as the line force during the downward stroke. Meanwhile, the translator weight, which can be seen as the average no load force within the full active area, will always weigh downwards and the friction force will work opposite the direction of movement. The friction force is further studied in Section 3.2.2.

The difference in line force, between each load case and the corresponding no load case, in both Figures 5 and 6, show the PTO force going into the generator. The PTO force is studied further in Section 3.3.

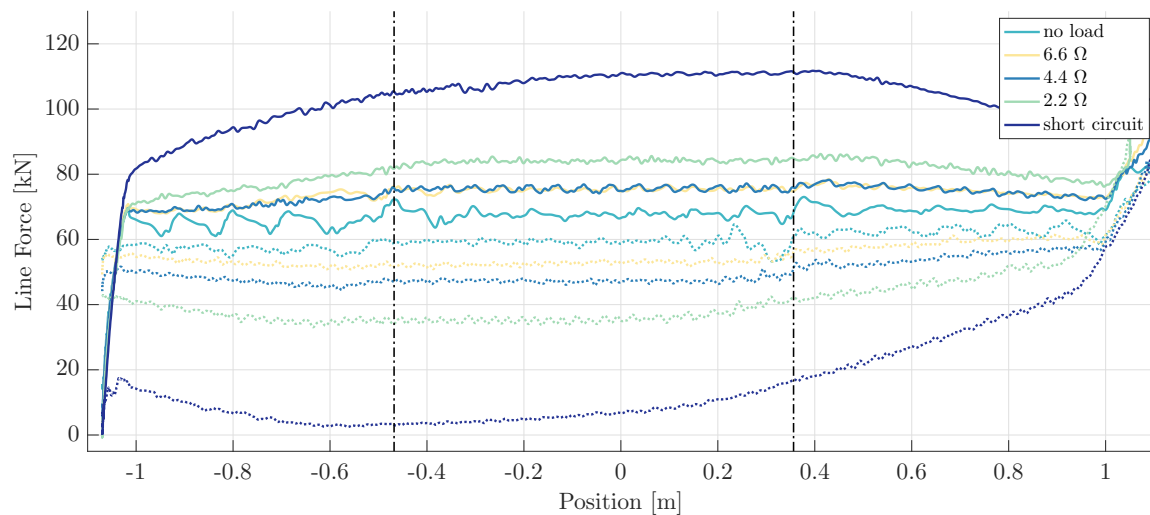


Figure 5. Line force in position domain for the low speed tests. Upward motion is represented with solid lines and downward motion is represented with dotted lines. The full active area is marked by vertical dotted lines.

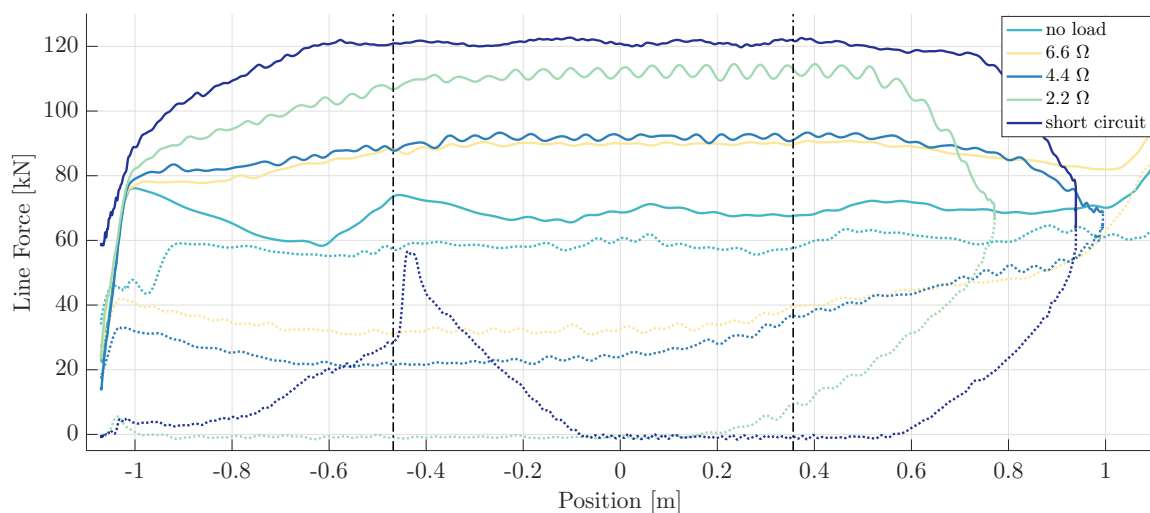


Figure 6. Line force in position domain for the high speed tests. Upward motion is represented with solid lines and downward motion is represented with dotted lines. The full active area is marked by vertical dotted lines.

3.2.1. Oscillations

The no load force, in both time and position domain, see Figures 2a, 3a, 5 and 6, shows strong oscillations during the upward and downward strokes. This is also seen in the uneven speed in Figures 2b and 3b. The period of this oscillation, when measured in either time or distance, varies between slow and fast strokes. It can be observed that the oscillations start strong and then subside, which suggest an impulse oscillation due to spring effect in the jib. This type of oscillations are not to be expected during offshore operation, since the buoy line has a very low elasticity.

Smaller and more consistent oscillations can be seen in the 2.2 Ω, 4.4 Ω and 6.6 Ω cases, seen in Figures 2a, 3a, 5 and 6. The period measured in distance corresponds to one magnetic pole-width, for both the slow and the fast stroke. This suggests that these oscillations are distance dependent, probably due to cogging in the generator. Cogging is to be expected during operation, even though the winding pattern of the stator has been designed to reduce it as much as possible. It should not affect the power production significantly, but will cause wear on the WEC.

3.2.2. Losses at No Load

By using Equation (4) for the no load case, presented in Figures 5 and 6, the no load loss was calculated to 4.15 kN for the slow stroke, at 0.1 m/s, and to 4.84 kN for the fast stroke, at 0.4 m/s. This is a sum of the friction and the iron losses at no load. The iron losses depend on both electrical frequency and load, and should be small in the no load case [26], suggesting that the measured loss mainly derives from friction. A speed dependence of the friction is expected, and the measured loss supports this. The experiment presented in this paper does not, however, provide enough data to further analyze the speed dependence.

3.3. PTO Force and Damping

The PTO force, presented in Figure 7a, was calculated from the line force measurements, using Equations (2) and (3) and subtracting the no load loss. The speed, derived from the translator position, is plotted in Figure 7b. By normalizing the PTO force with translator speed, the damping factor γ is obtained and presented in Figure 7c. The values for γ during the full active area for both upward and downward strokes for the low speed cases, are presented in Table 5. In the no load case, for which the γ value is expected to be zero since no power is produced by the generator, a γ value of almost 10 kNs/m was found for both the upward and downward strokes.

It can be seen that γ decreases linearly with a decreasing active area, as the translator moves outside the vertical dotted lines in Figure 7c. The slope varies with load case; a higher load gives a stronger inclination. As the translator moves from the full active area to the upper endstop, γ drops in the range of 39% to 53% for the different load cases. It can also be seen that the γ value during the partial active area is higher when the translator leaves the stator, and lower when it enters the stator.

Table 5. The damping factor γ at full stator overlap for each load case used in the low speed tests.

Load Case	PTO Damping Factor, γ Upward Stroke	PTO Damping Factor, γ Downward Stroke
short circuit	440 kNs/m	440 kNs/m
2.2 Ω	185 kNs/m	185 kNs/m
4.4 Ω	95 kNs/m	85 kNs/m
6.6 Ω	80 kNs/m	40 kNs/m

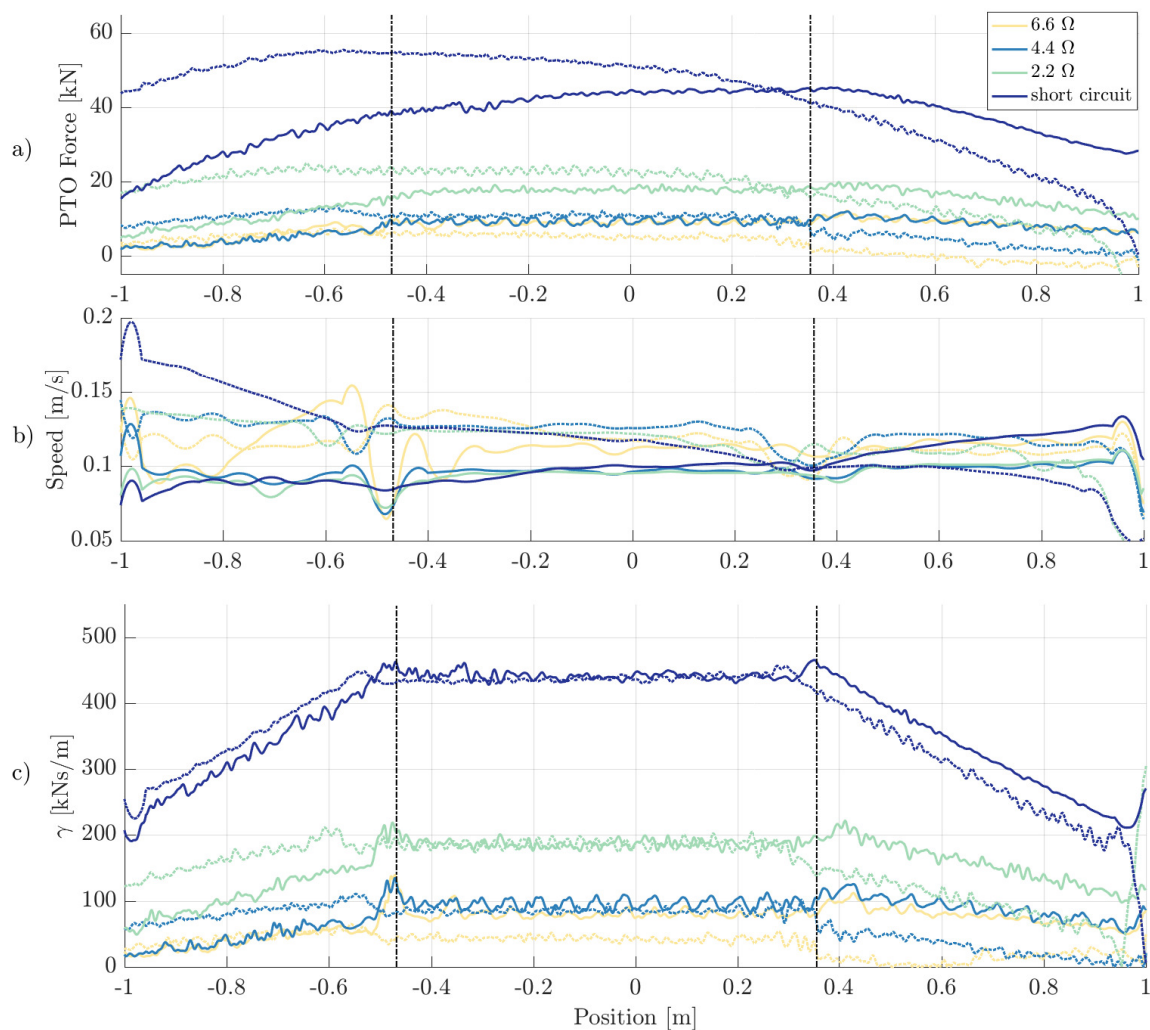


Figure 7. PTO force (a), translator speed (b) and PTO damping, γ , (c) for the low speed stroke. The upward motion is represented with solid lines and the downward motion is represented with dotted lines. The full active area is marked by vertical dotted lines.

4. Discussion

As was seen in Figures 2 and 3 and in Table 5, an increased PTO damping gave an increased endstop force. This result differs from the results from tank tests presented in reference [20], where an increased damping resulted in decreased peak forces. The difference between the results can be understood and is expected since the crane is operated to provide a constant speed, while in tank tests, the wave lifts the buoy with a time-varying instantaneous power, and the speed of the buoy depends on both the wave and the generator characteristics such as PTO damping. The results presented here provide a new insight into the tank tests presented in [20]; there, the decreased peak forces are an implication of the decreased translator speed and retardation, which, in turn, is an effect of the increased PTO damping.

In [21], the power production of an earlier WEC prototype, which is similar but with a lighter translator, was studied. It was found that the output power was higher during the upward motion than during the downward motion. It was suggested that a higher translator weight would give a higher and more evenly distributed power output. The onshore experiments in this study do not provide enough data to analyze the power production within a wider speed range. Even so, comparing γ values when lifting and lowering the translator does confirm a good balance between the upward and downward stroke at the speeds tested. It should be noted, however, that the generator is expected

to operate also at higher speeds during offshore operation. From the translator speed during free-fall, in the 2.2 Ω case presented in Figure 3, it can be concluded that 2.2 Ω is not a suitable load for this generator during offshore operation at rated speed, since the translator will not move fast enough to return to the bottom position in the wave troughs. Using loads that are too high may result in a lower and less balanced power production, as was seen in [21]. Furthermore, this may cause unwanted snatch loads, since there will be line-slack between translator and buoy.

The γ values at full active area were found constant and very similar in value for both upward and downward strokes, except for the 6.6 Ω case, which shows a larger γ value during upward motion. In addition, a small but non-negligible γ value for the no load case was found. Possible explanations could be that the translator weight measure was incorrect or that the generator shows different friction losses during upward and downward strokes. As the translator leaves the full active area region, marked with dotted lines in Figure 7, there are local disturbances in both γ and speed. These are due to linear generator end effects, which have previously been studied in [28]. These electromagnetic effects, due to the non-symmetric design of a linear generator, also contribute to cogging, which was seen as force and speed oscillations during the experiment.

The linear decrease in γ with decreased A_{fac} was measured, and it was seen that the slope varied with load case; a higher PTO-damping resulted in a larger drop of the PTO-damping when the active area decreased. During offshore operation, this would mean that the damping would decrease as the translator moves towards the endstop and the translator speed would increase, thus increasing the endstop force. It would be of interest for future work to investigate how this load dependence would influence the damaging forces during offshore operation.

In Section 3.2.2, the losses at no load were calculated for two different speeds. When increasing the speed from 0.1 m/s to 0.4 m/s, the losses increased approximately 14%. The no load loss is a sum of friction and iron loss, where the iron loss should be small at no load. The friction force is partly due to roll friction from the wheel-tracks, along which the translator is moving, and the mechanical lead-through system where the buoy line force is guided into the generator. The former is expected to increase with higher speeds, while the latter should decrease with higher speeds. From the result of only two studied speeds, little can be said about the expected friction losses during offshore operation, but it can be concluded that friction forces are to be expected and that they will vary with speed.

5. Conclusions

Line force and the generator damping coefficient γ have been studied for the full stroke of a linear generator, including full stator overlap, partial overlap and at endstop impact, when connected to five different load cases: no load, 6.6 Ω , 4.4 Ω , 2.2 Ω and short circuited. It was seen that a higher damping gives a higher line force and higher upper endstop force. The damping factor γ was calculated for each load case, showing a constant γ during the full active area and linearly decreasing γ when leaving full stator overlap. It could be seen that the γ drop was larger for cases with higher damping. It was also seen that the γ value during the partial active area is higher when leaving the stator, and lower when entering the stator. For future work, a deeper analytical study of the relationship between stator overlap and generator damping is suggested, together with extended onshore tests. It should also be studied how this behavior affects energy yield and unwanted forces during offshore operation.

Finally, it could be confirmed that an increased translator weight, as suggested when studying earlier prototypes, improves the speed, damping and power takeoff balance between the upward and the downward strokes. It was also seen that short circuiting the generator will lead to a near translator standstill during the downward stroke, and that a 2.2 Ω load, which was used previously during offshore experiments, will limit the speed 0.35 m/s during the downward stroke.

Acknowledgments: The work was supported by Vargöns Research Foundation, the Swedish Research Council Grant No. 621-2009-3417, the Centre for Natural Disaster Science (CNDS) in Sweden, the Swedish Energy Agency, Vinnova and Seabased Industry AB.

Author Contributions: L.U. and L.S. conceived and designed the experiments; L.U. performed the experiments and analyzed the data; M.L. provided the experiment facilities; L.U., L.S. and M.G. wrote the paper.

Conflicts of Interest: The authors declare no conflict of interest.

Abbreviations

The following abbreviations are used in this manuscript:

WEC Wave Energy Converter
 FFT Fast Fourier Transform
 PTO Power Take-Off

References

1. Drew, B.; Plummer, A.; Sahinkaya, M. A review of wave energy converter technologies. *Proc. Inst. Mech. Eng. Part A J. Power Energy* **2009**, *223*, 887–902.
2. Falcao, A. Wave Energy Utilization: A review of the technologies. *Renew. Sustain. Energy Rev.* **2010**, *14*, 899–918.
3. Mueller, M. Electrical generator for direct drive wave energy converters. *IEEE Proc. Gener. Transm. Distrib.* **2002**, *149*, 446–456.
4. Salter, S.; Taylor, J.; Caldwell, N. Power conversion mechanisms for wave energy. *J. Eng. Marit. Environ.* **2002**, *218*, 1–27.
5. Polinder, H.; Damen, M.; Gardner, F. Linear generator system for wave energy conversion in the AWS. *IEEE Trans. Energy Convers.* **2004**, *19*, 583–589.
6. Polinder, H.; Jack, B.M.A.; Dickinson, P.; Mueller, M. Conventional and TFPM linear generators for direct-drive wave energy conversion. *IEEE Trans. Energy Convers.* **2005**, *20*, 260–267.
7. Guiberteau, K.; Lee, J.; Liu, Y.; Dou, Y.; Kozman, T. Wave energy converters and design considerations for gulf of Mexico. *Distrib. Gener. Altern. Energy J.* **2015**, *30*, 55–76.
8. Pastor, J.; Liu, Y. Power absorption modeling and optimization of a point absorbing wave energy converter using numerical method. *ASME J. Energy Resour. Technol.* **2014**, *136*, 021207.
9. Pastor, J.; Liu, Y. Frequency and time domain modeling and power output for a heaving point absorber wave energy converter. *Int. J. Energy Environ. Eng.* **2014**, *5*, 101.
10. Leijon, M.; Waters, R.; Rahm, M.; Svensson, O.; Bodström, C.; Strömstedt, E.; Engström, J.; Tyrberg, S.; Savin, A.; Gravråkmö, H.; et al. Catch the wave to electricity. *IEEE Power Energy Mag.* **2009**, *7*, doi:10.1109/MPE.2008.930658.
11. Eriksson, M.; Waters, R.; Svensson, O.; Isberg, J.; Leijon, M. Wave power absorption: Experiments in open sea and simulation. *J. Appl. Phys.* **2007**, *102*, 084910.
12. Boström, C.; Svensson, O.; Rahm, M.; Lejerskog, E.; Savin, A.; Strömstedt, E.; Engström, J.; Gravråkmö, H.; Haikonen, K.; Waters, R.; et al. Design Proposal of Electric System for Linear Generator Wave Power Plants. In Proceedings of the IEEE Industrial Electronics IECON2009, Porto, Portugal, 3–5 November 2009.
13. Danielsson, O. Wave energy conversion—Linear synchronous permanent magnet generator. Ph.D. Thesis, Uppsala University, Uppsala, Sweden, 20 October 2006.
14. Sjökvist, L.; Krishna, R.; Castellucci, V.; Hagnestål, A.; Rahm, M.; Leijon, M. On the Optimization of Point Absorber Buoys. *J. Mar. Sci. Eng.* **2014**, *2*, 477–492.
15. Gravråkmö, H.; Strömstedt, E.; Savin, A.; Leijon, M. Measurements of Extreme Forces on a Wave Energy Converter of Point Absorber Type and Estimation of Added Mass of Cylindrical Buoy. In Proceedings of the ASME 2014 33rd International Conference on Ocean, Offshore and Arctic Engineering, OMAE, San Francisco, CA, USA, 8–13 June 2014.
16. Waters, R.; Rahm, M.; Eriksson, M.; Svensson, O.; Strömstedt, E.; Boström, C.; Sundberg, J.; Leijon, M. Ocean wave energy absorption in response to wave period and amplitude offshore experiments on a wave energy converter. *IET Renew. Power Gener.* **2011**, *5*, 465–469.
17. Leijon, M.; Bodström, C.; Danielsson, O.; Gustafsson, S.; Haikonen, K.; Langhamer, O.; Strömstedt, E.; Stalberg, M.; Sundberg, J.; Svensson, O.; et al. Wave energy from the North Sea: Experiences from the Lysekil research site. *Surv. Geophys.* **2008**, *29*, 221–240.

18. Savin, A.; Svensson, O.; Strömstedt, E.; Boström, C.; Leijon, M. Determining the Service Life of a Steel Wire Under a Working Load in the Wave Energy Converter. In Proceedings of the ASME 28th International Conference on Ocean, Offshore and Arctic Engineering, OMAE 2009, Honolulu, HI, USA, 31 May–5 June 2009.
19. Svensson, O.; Leijon, M. Peak force measurements on a cylindrical buoy with limited elastic mooring. *IEEE J. Ocean. Eng.* **2014**, *39*, 398–403.
20. Göteman, M.; Engström, J.; Eriksson, M.; Leijon, M.; Hann, M.; Ransley, E.; Greaves, D. Wave loads on a point-absorbing wave energy device in extreme waves. *J. Ocean Wind Energy* **2015**, *2*, 176–181.
21. Lejerskog, E.; Boström, C.; Hai, L.; Waters, R.; Leijon, M. Experimental results on power absorption from a wave energy converter at the Lysekil wave energy research site. *Renew. Energy* **2015**, *77*, 9–14.
22. Stalberg, M.; Waters, R.; Danielsson, O.; Leijon, M. Influence of generator damping on peak power for a direct drive wave energy converter. *J. Offshore Mech. Arct. Eng.* **2008**, *130*, 031003.
23. Rahm, M.; Svensson, O.; Bodström, C.; Waters, R.; Leijon, M. Experimental results from the operation of aggregated wave energy converters. *IET Renew. Power Gener.* **2012**, *6*, 149–160.
24. Mueller, M.; Polinder, H. *Electrical Drives for Direct Drive Renewable Energy Systems*; Woodhead Publishing: Cambridge, UK, 2013.
25. Czichos, H. *Tribology, A Systems Approach to the Science and Technology of Friction, Lubrication and Wear*; Elsevier: Amsterdam, The Netherlands; Oxford, UK; New York, NY, USA, 1975.
26. Shek, J.K.H.; Macpherson, D.E.; Mueller, M.A.; Xiang, J. Reaction force control of a linear electrical generator for direct drive wave energy converter. *Renew. Power Gener.* **2007**, *1*, 17–24.
27. Castellucci, V.; Abrahamsson, J.; Svensson, O.; Waters, R. Algorithm for the calculation of the translator position in permanent magnet linear generators. *J. Renew. Sustain. Energy* **2014**, *6*, 063102.
28. Danielsson, O.; Leijon, M. Flux distribution in linear permanent-magnet synchronous machines including longitudinal end effects. *IEEE Trans. Magn.* **2007**, *43*, 3197–3201.



© 2016 by the authors; licensee MDPI, Basel, Switzerland. This article is an open access article distributed under the terms and conditions of the Creative Commons Attribution (CC-BY) license (<http://creativecommons.org/licenses/by/4.0/>).